Atmos. Chem. Phys., 23, 2379–2391, 2023
https://doi.org/10.5194/acp-23-2379-2023

Atmospheric Chemistry and Physics
Open Access
EGU

Research article

Elucidate the formation mechanism of particulate nitrate based on direct radical observations in the Yangtze River Delta summer 2019

Tianyu Zhai[1], Keding Lu[1,2], Haichao Wang[3], Shengrong Lou[4], Xiaorui Chen[1,a], Renzhi Hu[5], and Yuanhang Zhang[1,2]

[1]State Key Joint Laboratory of Environmental Simulation and Pollution Control, College of Environmental Sciences and Engineering, Peking University, Beijing 100871, China
[2]Collaborative Innovation Center of Atmospheric Environment and Equipment Technology, Nanjing University of Information Science & Technology, Nanjing 210044, China
[3]School of Atmospheric Sciences, Sun Yat-sen University, Guangzhou 510275, China
[4]State Environmental Protection Key Laboratory of Formation and Prevention of the Urban Air Complex, Shanghai Academy of Environmental Sciences, Shanghai 200223, China
[5]Key Laboratory of Environmental Optics and Technology, Anhui Institute of Optics and Fine Mechanics, Chinese Academy of Sciences, Hefei 230031, China
[a]now at: Department of Civil and Environmental Engineering, Hong Kong Polytechnic University, Hong Kong, China

Correspondence: Keding Lu (k.lu@pku.edu.cn) and Yuanhang Zhang (yhzhang@pku.edu.cn)

Received: 7 August 2022 – Discussion started: 12 August 2022
Revised: 20 December 2022 – Accepted: 11 January 2023 – Published: 21 February 2023

Abstract. Particulate nitrate (NO_3^-) is one of the dominant components of fine particles in China, especially during pollution episodes, and has a significant impact on human health, air quality, and climate. Here a comprehensive field campaign that focuses on the atmospheric oxidation capacity and aerosol formation and their effects in the Yangtze River Delta (YRD) was conducted from May to June 2019 at a regional site in Changzhou, Jiangsu Province in China. The concentrations of NO_3^-, OH radicals, N_2O_5, NO_2, O_3, and relevant parameters were measured simultaneously. We showed a high NO_3^- mass concentration with $10.6 \pm 8.9\,\mu g\,m^{-3}$ on average, which accounted for 38.3 % of total water-soluble particulate components and 32.0 % of total $PM_{2.5}$, followed by the proportion of sulfate, ammonium, and chloride by 26.0 %, 18.0 %, and 2.0 %, respectively. This result confirmed that the heavy nitrate pollution in eastern China happened not only in winter, but also in summer. This study's high nitrate oxidation ratio (NOR) emphasized the solid atmospheric oxidation and fast nitrate formation capacity in the YRD. It was found that $OH + NO_2$ during daytime dominated nitrate formation on clean days, while N_2O_5 hydrolysis vastly enhanced and became comparable with that of $OH + NO_2$ during polluted days (67.2 % and 30.2 %, respectively). The updated observed-constraint Empirical Kinetic Modeling Approach (EKMA) was used to assess the kinetic controlling factors of both local O_3 and NO_3^- productions, which indicated that the O_3-targeted scheme ($VOCs : NO_x = 2 : 1$) is adequate for mitigating the O_3 and nitrate pollution coordinately during summertime in this region. Our results promote the understanding of nitrate pollution mechanisms and mitigation based on field observation and model simulation and call for more attention to nitrate pollution in the summertime.

Published by Copernicus Publications on behalf of the European Geosciences Union.

1 Introduction

Chemical compositions of fine particles have been measured in China during the past 20 years, and secondary inorganic aerosol is regarded as one of the dominant species in aerosol (Cao et al., 2012; Hagler et al., 2006; Zhao et al., 2013; Andreae et al., 2008). Since the Air Pollution Prevention and Control Action Plan, there has been a significant decrease in SO_2, NO_2, and $PM_{2.5}$ concentrations in China, while the inorganic nitrate ratio in $PM_{2.5}$ increased and became the considerable component in $PM_{2.5}$ (Shang et al., 2021; Zhang et al., 2022). Therefore, a comprehensive understanding of the particulate nitrate formation mechanism is essential and critical for mitigating haze pollution in China.

Massive research has been done in China to investigate nitrate formation mechanisms, and a basic framework has been established (Sun et al., 2006; Chang et al., 2018; Wu et al., 2019). In the daytime, $NO_2 + OH$ radical oxidation (Reaction 1) is the major particulate nitrate formation pathway. The product (HNO_3) reacts with alkaline substances in aerosol, generating particulate nitrate. This pathway is mainly controlled by precursor concentrations as well as the gas-particle partition of gaseous nitric acid, and particulate nitrate depends on temperature, relative humidity (RH), NH_3 concentration, and aerosol acidity (Wang et al., 2009; Song and Carmichael, 2001; Meng et al., 2020; Zhang et al., 2021). At night, N_2O_5 uptake is a vital nitrate formation pathway (Reaction 4) (Chen et al., 2020; Wang et al., 2022). N_2O_5 is formed through $NO_2 + NO_3$ (Reaction 3), and there exists a quick thermal equilibrium balance ($K_{eq} = 5.5 \times 10^{-17}\,cm^{-3}\,molec.^{-1}\,s^{-1}$, 298 K). However, two problems remain ambiguous in quantifying the contribution of N_2O_5 uptake to nitrate formation. The first is that the N_2O_5 heterogeneous uptake coefficient (γ) on ambient aerosol is highly varied, with a range from 10^{-4} to 10^{-1} based on previous lab and field measurements (Bertram and Thornton, 2009; Brown et al., 2009; Z. Wang et al., 2017; Wang and Lu, 2016). The other one is the $ClNO_2$ production yield which influences nitrate contribution due to the extensive variation range (Phillips et al., 2016; Staudt et al., 2019; Tham et al., 2018). Both parameters are complex to well-predicted by current schemes. No_2 heterogeneous uptake has been found to be non-negligible for nitrate formation, which can be a vital pathway during heavy haze events according to recent studies (Qiu et al., 2019; Chan et al., 2021). The uptake coefficient and nitrate yield remain uncertain, as with the N_2O_5 heterogeneous reaction. In addition, N_2O_5 homogeneous hydrolysis and NO_3 radical oxidation have a minor contribution to particulate nitrate under ambient conditions (Brown et al., 2009; Seinfeld and Pandis, 2016).

$$NO_2 + OH \rightarrow HNO_3 \quad \text{(R1)}$$

$$NO_2 + O_3 \rightarrow NO_3 + O_2 \quad \text{(R2)}$$

$$NO_2 + NO_3 + M \rightarrow N_2O_5 + M \quad \text{(R3.1)}$$

$$N_2O_5 + M \rightarrow NO_2 + NO_3 + M \quad \text{(R3.2)}$$

$$N_2O_5 + (H_2O \text{ or } Cl^-) \rightarrow (2-\varphi)\,NO_3^- + \varphi ClNO_2 \quad \text{(R4)}$$

As a critical area of China's economy and industry, the Yangtze River Delta (YRD) has suffered severe air pollution during past decades, and fine particle pollution in the YRD has raised widespread concern (Guo et al., 2014; Zhang et al., 2015, 2017; Ming et al., 2017; Xue et al., 2019). However, most research focuses on wintertime $PM_{2.5}$ pollution and lacks measurements of critical intermediate species and radicals to assess the importance of each nitrate formation pathway. In this study, with the direct measurements of hydroxyl radicals and the reactive nitrogen compounds and chemical box model analyses, we explore the characteristics of nitrate and precursors in the YRD in the summer of 2019, the importance of particulate nitrate formation pathways is quantified, and the controlling factors are explored. A further suggestion for summer pollution prevention and control in the local area is proposed.

2 Site description and methods

2.1 The campaign site

This campaign took place at a suburban sanatorium from 30 May to 18 June 2019 in Changzhou, China. Changzhou (119.95° E, 31.79° N) is located in Jiangsu Province and about 150 km northwest of Shanghai. The sanatorium, located 420 m east of Lake Ge (one of the largest lakes in Jiangsu Province, 164 km^2), is surrounded by farmland and fishponds. With the closest arterial traffic 1 km away, several industry zones are 4 km to the east. The prevailing wind was from the southern and southeastern sectors (about 30 % of the time) compared to 20 % from the western sector, of which only 15 % came from the east. The wind speed was usually lower than 5 m s^{-1}, with faster speed from the west. This site was influenced by anthropogenic and biological sources with occasional biomass burning.

2.2 The instrumentation

Multiple gaseous and particulate parameters were measured simultaneously during the campaign to comprehensively interpret the nocturnal atmospheric capacity and aerosol formation. The related instruments are listed in Table 1. N_2O_5 and particle number and size distribution (PNSD) were measured on the fourth floor of the sanatorium, which is the top of the building. Other instruments were placed in containers on the ground 170 m northeast of the building and sampling

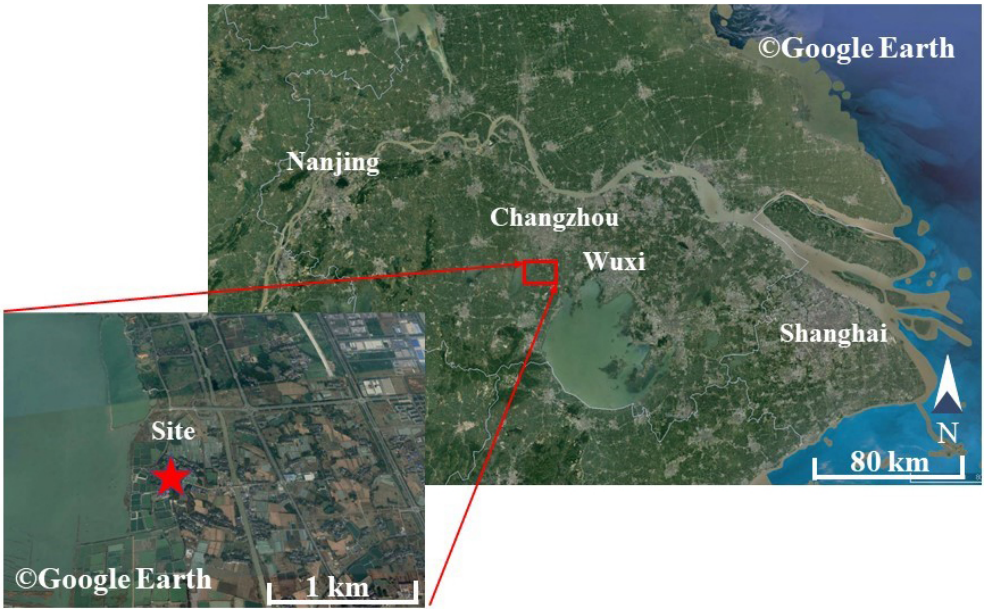

Figure 1. The location of the campaign site (red star), Changzhou, is 150 km on the northwestern side of Shanghai.

inlets at circa 5 m above the ground through the containers' roof.

N_2O_5 was measured by a cavity-enhanced absorption spectrometer (CEAS) based on the Lambert–Beer law which was developed by Wang et al. (2017b). Briefly, air samples were drawn through the window and reached out of the wall 30 cm to prevent influence from surface deposition. The aerosol membrane filter was deployed before the perfluoroalkoxy alkane (PFA) sampling tube and changed every 2 h at night to avoid a decrease in N_2O_5 transmission efficiency due to the increased loss of N_2O_5 from the accumulated aerosols on the filter. N_2O_5 was decomposed into NO_3 and NO_2 by preheating tube heat at 130° and detected within a PFA-coated resonator cavity heated at 110° to prevent the formation of N_2O_5 by reversible reaction subsequently. At the end of each sampling cycle (5 min), a 30 s injection of high-concentration NO (10 ppm, 20 mL min^{-1}) mixed with sample air was set to eliminate NO_3–N_2O_5 from the system. The NO titration spectra were adopted as the dynamic background spectrum by assuming no H_2O concentration variation in a single sampling cycle. The loss of N_2O_5 in the sampling system and filter was also considered during data correction. The limit of detection (LOD) was estimated to be 2.7 pptv (1σ) with an uncertainty of 19 %.

OH radical measurement was conducted by fluorescence assay by gas expansion laser-induced fluorescence techniques (FAGE-LIF). Ambient air was expanded through a 0.4 mm nozzle to low pressure in a detection chamber, where the 308 nm laser pulse irradiated OH radicals at a repetition rate of 8.5 kHz (Chen et al., 2018). NO_x and O_3 were monitored by commercial monitors (Thermo-Fisher 42i and 49i). Volatile organic compounds (VOCs) were measured by an automated gas chromatograph equipped with a mass spectrometer and flame ionization detector (GC-MS) with a time resolution of 60 min. The photolysis frequencies were determined from the spectral actinic photon flux density measured by a spectroradiometer (Bohn et al., 2008).

$PM_{2.5}$ concentration was obtained by a Tapered Element Oscillating Microbalance (TEOM 1405, Thermo Scientific Inc). Aerosol surface concentration (S_a) was converted from the particle number and size distribution, which was measured by a Scanning Mobility Particle Sizer (SMPS, TSI 3936) and an Aerosol Particle Sizer (APS, TSI 3321) and modified to the wet particle-state S_a with a hygroscopic growth factor (Liu et al., 2013). The uncertainty of the wet S_a was $\sim$ 30 %. Meanwhile, water-soluble particulate components and their gaseous precursors were analyzed through the Monitor for AeRosols and GAses in ambient air (MARGA, Chen et al., 2017). Meteorological data were also available, including the temperature, RH, pressure, wind speed, and wind direction.

2.3 The Empirical Kinetic Modeling Approach

A box model coupled with the Regional Atmospheric Chemical Mechanism version 2 (RACM2, Goliff, Stockwell and Lawson, 2013) is used to conduct the mitigation strategy studies. The model is operated at 1 h time resolution with measurement results of temperature, relative humidity, pressure, CO, NO_2, H_2O, photolysis frequencies, and aggregated VOC input to constrain the model. It should be noted that HONO concentration is calculated by $NO_2 \times 0.02$, as suggested by Elshorbany et al. (2012), and has been used in the box model before (Lou et al., 2022). Long-lived species

Table 1. The observed gas and particle parameters during the campaign.

Parameters	Detection of limit	Method	Accuracy
N_2O_5	2.7 pptv (1σ, 1 min)	CEAS	±19 %
OH	1.6×10^5 cm^{-3} (1σ, 60 s)	LIF[a]	±21 %
NO	60 pptv (2σ, 1 min)	PC[c]	±10 %
NO_2	0.3 ppbv (2σ, 1 min)	PC[c]	±10 %
O_3	0.5 ppbv (2σ, 1 min)	UV photometry	±5 %
VOCs	20–300 pptv (60 min)	GC-MS	±15 %
$PM_{2.5}$	0.1 µg m^{-3} (1 min)	TEOM[d]	±5 %
Photolysis frequencies	5×10^{-5} s^{-1} (1 min)	SR[e]	±10 %
PNSD	14–700 nm (4 min)	SMPS, APS	±10 %
HNO_3, NO_3, HCl	0.06 ppbv (30 min)	MARGA[f]	±20 %
NH_4^+, NO_3^-, Cl^-, SO_4^{2-}	0.05 µg m^{-3} (30 min)	MARGA[f]	±20 %

[a] Laser-induced fluorescence. [b] Chemiluminescence. [c] Photolytic converter. [d] Tapered Element Oscillating Microbalance. [e] Spectroradiometer. [f] The Monitor for AeRosols and GAses in ambient air.

such as H_2 and CH_4 are assumed to be constants (550 and 1900 ppbv, respectively). Moreover, a 13 h constant loss rate of unconstrained intermediate and secondary products, the result of synthetic evaluating secondary simulation of secondary species, is set for representing the multiple effects of deposition, transformation, and transportation.

The approaches to the chemical production of O_3 ($P(O_3)$) and inorganic nitrate ($P(NO_3^-)$) are described in previous articles (Tan et al., 2021, 2018) and expressed as Eqs. (1) and (4).

$$P(O_3) = F(O_3) - D(O_3) \quad (1)$$

$$F(O_3) = k_{HO_2+NO}[NO][HO_2] + k_{(RO_2+NO)eff}[NO][RO_2] \quad (2)$$

$$D(O_3) = k_{OH+NO_2}[OH][NO_2] + (k_{OH+O_3}[OH] + k_{HO_2+O_3}[HO_2] + k_{alkenes+O_3}[alkenes])[O_3] \quad (3)$$

$$P(NO_3^-) = P(HNO_3) + P(pNO_3^-) \quad (4)$$

$$P(HNO_3) = k_{OH+NO_2}[OH][NO_2] \quad (5)$$

$$P\left(pNO_3^-\right) = 0.25(2-\varphi)C\gamma_{S_a}[N_2O_5] \quad (6)$$

Briefly, $P(O_3)$ is net ozone production, which is calculated by peroxyl radial + NO oxidation (Eq. 2) minus the chemical loss of O_3 and NO_2 (Eq. 3). $P(NO_3^-)$ is constituted by reaction $OH + NO_2$ (Eq. 5) and N_2O_5 heterogeneous uptake (Eq. 6). Here, rate constants of reactions are obtained from the NASA JPL publication or RACM2 (Goliff et al., 2013). γ is the N_2O_5 uptake coefficient calculated from parameterization (γ_P; more details in Sect. 3.3). φ represents $ClNO_2$ production yield through N_2O_5 hydrolysis, and the mean value reported by Xia et al. (2020) is used in this work.

The Empirical Kinetic Modeling Approach (EKMA) was invented to study the effects of precursor (VOC and NO_x) reactivity on the region's ozone pollution by Kanaya et al. (2008) and helps recognize the region's susceptibility to precursors by weight and became a prevalent tool to study the process of ozone formation (Tan et al., 2018; D. Yu et al., 2020; Kanaya et al., 2008). The prevention and control problem of pollutant generation can be transformed through the EKMA curve to reduce its precursors' emissions. Furthermore, the precursor reduction scheme needed for total pollutant control is given qualitatively. $P(NO_3^-)$ can also be analyzed through EKMA for the nonlinear secondary formation relationship with precursor reactivity. Here, an isopleth diagram of the net ozone production rate as functions of the reactivities of NO_x and VOCs can be derived from EKMA. In detail, 0.01 to 1.2 emission reduction strategy assumptions are exponentially interpolated into 20 kinds of emission situations of NO_x and VOCs, respectively, which counts 400 scenarios.

2.4 The calculation of aerosol liquid water content

Aerosol liquid water content (ALWC) is calculated through ISORROPIA II (Fountoukis and Nenes, 2007). Forward mode is applied in this study. Furthermore, water-soluble particulate components in $PM_{2.5}$ and gaseous species ($NH_3 + HNO_3 + HCl$) obtained from MARGA, along with RH and T, are input as initial input. In addition, a metastable aerosol state is chosen due to high RH during this campaign.

3 Result and discussion

3.1 Overview of measurements

The time used in this study is China Standard Time (UTC + 8), and the local sunrise and sunset times during the campaign were around 17:00 and 19:00, respectively. The whole campaign period is divided into four $PM_{2.5}$ clean periods and four $PM_{2.5}$ polluted periods (9 out of 14 d; the latter polluted period days refer to $PM_{2.5}$ pollution except for a specified description) according to the Chinese National Air Quality Standard (CNAAQS) Grade I of daily $PM_{2.5}$ concentrations (< 35.0 µg m^{-3}). Figure 2 shows the meteorological

parameters and gas-phase and particulate species time series during the observation. During the campaign, the temperature was high; the maximum reached 34.5°, with an average of $25.1 \pm 3.7°$. RH changed drastically from 21 % to 88 %, with a mean value of 58.9 ± 14.0 %. The mean NO_2 concentration was 14.8 ± 9.5 ppbv. Meanwhile, the O_3 average was 54.6 ± 28.8 ppbv, exceeding CNAAQS Grade II for a maximum daily average of 8 h ozone ($160\,\mu g\,m^{-3}$) on 14 out of 19 d and exceeding $200\,\mu g\,m^{-3}$ on 6 d.

Daytime OH radicals ranged from 2×10^6 to 8×10^6 molec. cm^{-3} with a daily peak over 3×10^6 molec. cm^{-3}. Maximum OH radicals reached 8.18×10^6 molec. cm^{-3} in this campaign. Compared with other summertime OH radicals observed in China, the OH radical concentration at this site is relatively low but still on the same order of magnitude (Lu et al., 2012, 2013; Ma et al., 2022; Tan et al., 2017; Woodward-Massey et al., 2020; Yang et al., 2021). N_2O_5 mean concentration was 21.9 ± 39.8 pptv with a nocturnal average of 61.0 ± 63.1 pptv and a daily maximum of over 200 pptv on eight nights. The maximum concentration of N_2O_5 (477.2 pptv, 5 min resolution) appeared at 20:47 on 8 June. The average NO_3 radical production rate $P(NO_3)$ is 2.1 ± 1.4 ppbv h^{-1}, with nocturnal average $P(NO_3)$ 2.8 ± 1.6 ppbv h^{-1} and daytime $P(NO_3)$ 2.2 ± 1.4 ppbv h^{-1}. $P(NO_3)$ is about twice the documented value in Taizhou and the North China Plain (Wang et al., 2017a, 2018b, 2020a) but close to another result in the YRD before (Chen et al., 2019). The average $PM_{2.5}$ was $34.6 \pm 17.8\,\mu g\,m^{-3}$, with a maximum reach of $163.0\,\mu g\,m^{-3}$. The water-soluble particulate components of $PM_{2.5}$ are displayed as well. The average NO_3^- concentration was $10.6\,\mu g\,m^{-3}$, which accounts for the 38.3 % mass concentration of water-soluble particulate components and 32.0 % total $PM_{2.5}$, while the proportions of sulfate, ammonium, and chloride are 26.0 %, 18 %, and 2.0 %, respectively. To sum up, during the campaign period, the pollution of $PM_{2.5}$ would be generally exacerbated on high O_3 and NO_2 days. Precipitation occurred during four clean processes and receded pollutant concentration; otherwise, the pollution condition remained severe.

The mean diurnal variations (MDCs) of temperature, RH, NO_2, O_3, $P(NO_3)$, N_2O_5, OH radicals, and $PM_{2.5}$ in different air quality are shown in Fig. 3. The temperature, RH, and OH radical MDCs show indistinct differences between clean days (CDs) and polluted days (PDs). The MDC of NO_2 has two concentration peaks that appear at 06:00 and 21:00 on CDs, while on PDs, its peak appears at 20:00 and maintains a high level during the whole night. The O_3 diurnal pattern reflects a typical urban-influenced character with a maximum O_3 peak that lasts 3 h from 14:00 to 17:00, while the PD O_3 peak concentration is 1.2 higher than the CD O_3 peak concentration. $P(NO_3)$ grows after the O_3 peak, and the maximum $P(NO_3)$ shows at 19:00 with an average value of 1.7 ppbv h^{-1} on CDs. By contrast, the mean PD P(NO3) is 2.6 ppbv h^{-1}, and the maximum value reaches 4.7 ppbv h^{-1}. In contrast, the CD N_2O_5 has a higher average and maximum concentration than PDs, which suggests a faster removal process during PDs. $PM_{2.5}$ has a similar trend to $P(NO_3)$ and has a higher concentration during nighttime.

3.2 The evolution of nitrate pollution

Figure 4a shows the relationship between nitrate and sulfate with water-soluble particulate components. Nitrate positively correlates with total water-soluble particulate components, while the sulfate ratio has an inverse correlation. With $PM_{2.5}$ concentration increasing, nitrate proportion increases rapidly and keeps high weight at a heavy $PM_{2.5}$ period, while the sulfate ratio shows the opposite phenomenon. Once the mass concentration of the total water-soluble particulate component is over $30\,\mu g\,m^{-3}$, the mass fraction of nitrate in total water-soluble particulate components is up to 50 % on average. This result illustrates that particulate nitrate is one of the vital sources of explosive growth particulate matter.

To further assess the conversion capacity of nitrate and sulfate at this site, the sulfur oxidation ratio (SOR) and the nitrogen oxidation ratio (NOR) are used to indicate the secondary transformation ratio of SO_2 and NO_2, respectively (Sun et al., 2006). SOR and NOR are estimated using the formulae below:

$$\mathrm{SOR} = \frac{n\mathrm{SO_4^{2-}}}{n\mathrm{SO_4^{2-}} + n\mathrm{SO_2}}, \tag{7}$$

$$\mathrm{NOR} = \frac{n\mathrm{NO_3^-}}{n\mathrm{NO_3^-} + n\mathrm{NO_2}}. \tag{8}$$

n refers to the molar concentration, and the higher SOR and NOR represent more oxidation of gaseous species into a secondary aerosol. As depicted in Fig. 4b–c, NOR rapidly increases at RH < 45 %, remains constant at 45 % < RH < 75 %, and ends with a sharp increase at RH > 75 %. During the study period, not only is the average concentration of NO_2 higher among PDs, but there is also a significant difference between PD and CD NOR. The average values of NOR are 0.32 on PDs and 0.25 on CDs, respectively, which manifests in the more secondary transformation and pollution potential on PDs. In contrast, the SOR stays constant at a high value (~ 0.5) during the whole RH scale, which shows a different pattern from previous research (Li et al., 2017; Zheng et al., 2015). One possible explanation is that SO_2 concentration stays low during the whole campaign (4.4 ± 2.4 ppbv on average), and SO_2 oxidation depends on the limit of SO_2 instead of oxidation capability. Meanwhile, the mean SOR in both situations is over 0.5 (0.52 on CDs and 0.56 on PDs), further supporting the SO_2-limited hypothesis. In addition, Table 2 summarizes NOR and SOR values in the YRD. NOR and SOR in this study are similar to values reported in other YRD research (Shu et al., 2019; Y. Zhang et

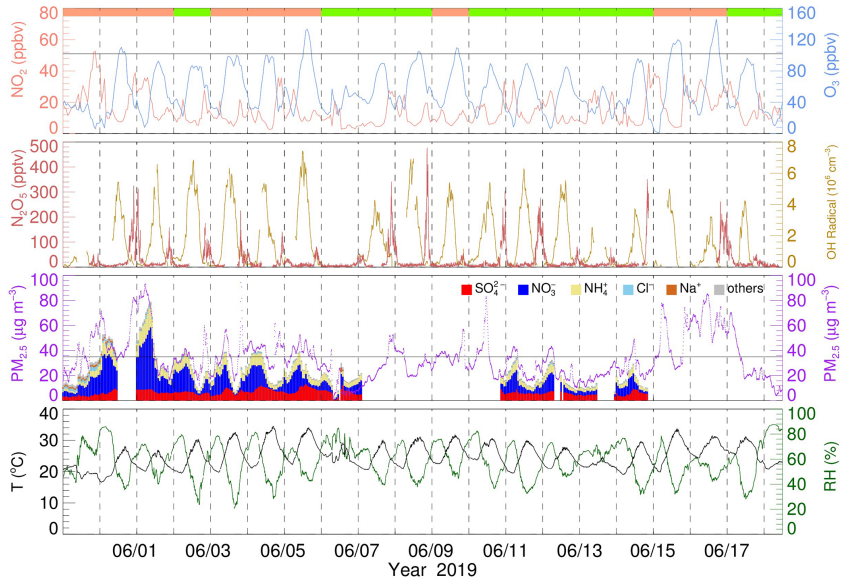

Figure 2. Time series of NO_2, O_3, N_2O_5, OH radicals, $PM_{2.5}$, and water-soluble particulate components, temperature, and RH. The vertical dotted line represents the zero clock. The black horizontal solid line in the O_3 and $PM_{2.5}$ panels represents Chinese national air quality standards for O_3 and $PM_{2.5}$, respectively. The top panel color blocks represent the $PM_{2.5}$ clean day (light green) and $PM_{2.5}$ polluted day (salmon).

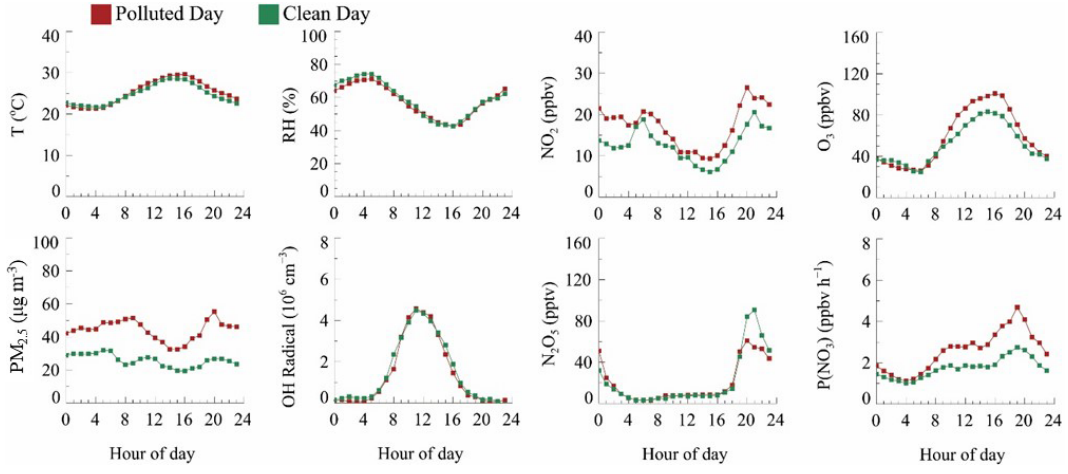

Figure 3. The mean diurnal variations of temperature, RH, NO_2, O_3, $PM_{2.5}$, OH radicals (orange), N_2O_5, and $P(NO_3)$ of clean days and polluted days.

al., 2020; Qin et al., 2021; Zhao et al., 2022), except for values in 2013, but higher than the North China study which emphasizes the solid atmospheric oxidation capacity in the YRD region.

3.3 The derivation of the N_2O_5 uptake coefficient

Statistical analysis of the observation above highlights the rapid formation of particulate nitrate. To assess the contribution of N_2O_5 hydrolysis to particulate nitrate formation, two methods are applied to calculate the N_2O_5 uptake coefficient. The first method is a stationary-state approximation (Brown et al., 2003). By assuming that the rates of production and loss of N_2O_5 are approximately in balance, the total loss rate of N_2O_5 ($k_{N_2O_5}$) can be calculated through Eq. (9). $k_{N_2O_5}$ is mainly dominated by N_2O_5 heterogeneous uptake, since homogeneous hydrolysis of N_2O_5 contributes little (Brown and Stutz, 2012). The N_2O_5 uptake coefficient through the steady state (denoted as γ_S) is derived as Eq. (10). Here C is the mean molecular speed of N_2O_5, and S_a is the aerosol surface concentration.

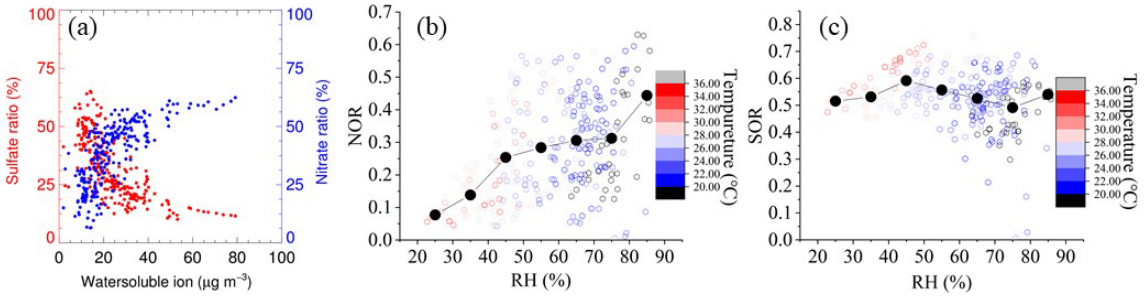

Figure 4. **(a)** Particulate ion mass concentration ratio of nitrate and sulfate to water-soluble ion. **(b)** NOR against RH, colored with temperature. **(c)** SOR against RH, colored with temperature.

Table 2. Statistical result of NOR and SOR in the YRD.

Location and year	SOR				NOR				References
	Max	Min	Mean	SD	Max	Min	Mean	SD	
Nanjing 2013 winter	0.42	0.10	0.28	0.11	0.29	0.15	0.21	0.05	Wang et al. (2016)
Suzhou 2013 winter	0.41	0.15	0.27	0.11	0.30	0.06	0.16	0.08	
Lin'an 2013 winter	0.50	0.19	0.35	0.11	0.24	0.12	0.18	0.05	
Hangzhou 2013 winter	0.30	0.14	0.21	0.06	0.11	0.06	0.09	0.02	
Ningbo 2013 winter	0.35	0.09	0.21	0.11	0.23	0.03	0.11	0.07	
YRD 2016 summer	–	–	0.347	–	–	–	0.11	–	Shu et al. (2019)
YRD 2016 winter	–	–	0.247	–	–	–	0.15	–	
Nanjing 2019 spring	0.48	0.38	–	–	0.31	0.29	–	–	Qin et al. (2021)
Changzhou 2019 spring	0.35	0.3	–	–	0.27	0.23	–	–	
Changzhou 2019 winter	0.68	0.24	0.35	0.12	0.44	0.13	0.2	0.1	Zhang et al. (2020)
Changzhou 2019 summer	0.16	0.76	0.54	0.1	0.08	0.63	0.28	0.14	This work

$$\tau_{ss}(N_2O_5) = \frac{[N_2O_5]}{k_{R3.1}[NO_2][O_3]} = \left(k_{N_2O_5} + \frac{k_{NO_3}}{K_{eq}[NO_2]}\right)^{-1} \quad (9)$$

$$k_{N_2O_5} = 0.25C\,\gamma\_S\,S_a \quad (10)$$

Due to the fast variety of NO_3 loss rates from VOCs, the steady-state method has been unattainable under conditions affected by emission interferences. During the whole campaign, we only retrieve three valid fitting results. As shown in Fig. 5, the fitted γ_S ranged from 0.057 to 0.123, which is comparable with Taizhou (0.041, Wang et al., 2020a) and much higher than other results in China (C. Yu et al., 2020; Wang et al., 2018a, 2020b, 2017a). The calculated k_{NO_3} ranged from 0.002 to 0.16 s^{-1}, representing drastic VOC change during this campaign.

The other approach is the parameterization by C. Yu et al. (2020), which is depicted as follows.

$$\gamma\_P = \frac{4}{c}\frac{V_a}{S_a}K_H \times 3.0 \times 10^4 \times [H_2O] \left(1 - \frac{1}{\left(0.033 \times \frac{[H_2O]}{[NO_3^-]}\right) + 1 + \left(3.4 \times \frac{[Cl^-]}{[NO_3^-]}\right)}\right) \quad (11)$$

V_a/S_a is the measured aerosol volume–surface area ratio by the SMPS, K_H is Henry's law coefficient, which is set to 51 as recommended, $[NO_3^-]$ and $[Cl^-]$ are aerosol inorganic concentrations measured by MARGA, and $[H_2O]$ is aerosol water content calculated by ISORROPIA II. The valid parameterization-calculated N_2O_5 uptake coefficient (denoted as γ_P) from 30 May to 8 June 2019 shows in Fig. 6 a good consistency between the trends of γ_P and aerosol water content. Nighttime γ_P varies from 0.001 to 0.024 with an average of 0.069 ± 0.0050 under polluted conditions and 0.0036 ± 0.0026 under clean conditions. The N_2O_5 uptake coefficient shows a good correlation between RH and aerosol water content. For the N_2O_5 uptake coefficient, al-

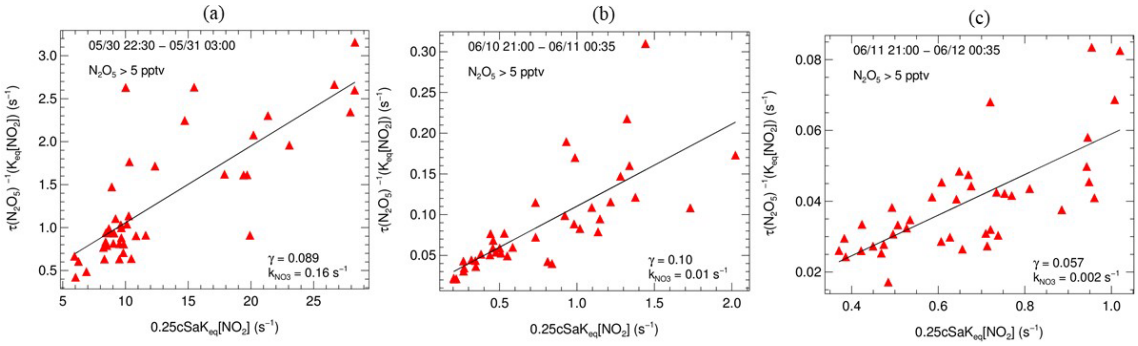

Figure 5. Derived N_2O_5 uptake coefficients from N_2O_5 steady lifetime (γ_S) with NO_2 and S_a; plots **(a–c)** represent the linear fitting results on the nights of 30 May, 10 and 11 June, respectively.

though particulate nitrate mass concentration increased during the pollution event, an antagonistic effect on the N_2O_5 uptake coefficient was not obvious for the nitrate molarity decrease.

Furthermore, we compare the difference between γ_S and γ_P. Taking the night of 30 May as an example, γ_S is 0.089, while γ_P ranges from 0.024 to 0.057 with an average value of 0.013 ± 0.0051. The difference between steady state and parameterization is significant; one possible explanation is uncertainty for stationary-state approximation caused by local NO or VOC emission (Brown et al., 2009; Chen et al., 2022). Another reason is that the parameterization by C. Yu et al. (2020) ignores the impact of organic matter on the fine particles. The difference in aerosol composition between this work and C. Yu et al. (2020) may also bring uncertainty. Overall, γ_P will be chosen for the N_2O_5 heterogeneous uptake coefficient in later analysis and discussion.

3.4 Quantifying the contribution of nitrate formation pathways

After the N_2O_5 uptake coefficient is counted, nitrate production potential $P(NO_3^-)$ can be calculated. Here the N_2O_5 uptake coefficient is set to 0.036 on clean days and 0.069 on polluted days, respectively, which are the average values derived from parameterization. The production ratio of NO_3^- (by considering the $ClNO_2$ yield of 0.54) is set to 1.46 in the former study (Xia et al., 2020). Gas-particle distribution is considered by the result of the particulate nitrate and gas-phase nitrate by MARGA (input HNO_3/NO_3^- ratio to the model as the $OH + NO_2$ nitrate production rate). The NO_2 heterogeneous uptake coefficient is set to 5.8×10^{-6} depending on the report by Yu et al. (2021), which is the result of 70 % RH on urban grime.

The mean diurnal variations of the nitrate production potential of clean and polluted days are depicted in Fig. 7. The $OH + NO_2$ pathway shows no significate difference between clean and polluted days and dominates CD nitrate formation potential, since the levels of OH and NO_2 are less affected by the fine particle level. However, the rapid increase in the N_2O_5 heterogeneous uptake pathway on polluted days is fatal, and its peak formation rate at night over the $OH + NO_2$ pathway can be used to explain nighttime nitrate explosive growth.

As shown in Fig. 7c, $OH + NO_2$ dominates nitrate production on clean days, while the N_2O_5 uptake pathway only contributes $13.6\,\mu g\,m^{-3}$. On polluted days, the ability of N_2O_5 uptake grows quickly, reaching $50.1\,\mu g\,m^{-3}$, while the OH pathway does not change much. There is no distinct difference in the daytime pathway ($OH + NO_2$) between clean days and polluted days, while the nighttime pathway ratio rises from 38.1 % on clean days to 67.2 % on polluted days. NO_2 heterogeneous uptake increases from $0.93\,\mu g\,m^{-3}$ on clean days to $2.0\,\mu g\,m^{-3}$ on polluted days, but the contribution proportion does not change obviously. Both the higher N_2O_5 uptake coefficient and the higher S_a on polluted days increase the contribution of N_2O_5 hydrolysis to particulate nitrate under pollution conditions.

3.5 Mitigation strategies of particulate nitrate and ozone productions

We selected two pollution episodes (Episode I, 30 May 2019 00:00–2 June 2019 00:00, and IV, 14 June 2019 17:30–17 June 2019 12:00) to explore the mitigation way of ozone and nitrate pollution. Figure 8 shows the EKMA of $P(O_3)$ and $P(NO_3^-)$ of these two periods, O_3 located in the VOC-controlling area in the two pollution episodes, which is consistent with a previous YRD urban ozone sensitivity study (Jiang et al., 2018; K. Zhang et al., 2020; Xu et al., 2021). The best precursor reduction for O_3 is $VOC : NO_x = 2 : 1$, while nitrate is located in the transition area, which means either of the precursors' reductions will mitigate nitrate pollution. For the regional and complex air pollution characteristics in this region, a fine particle-targeting reduction scheme will aggravate O_3 pollution. In contrast, the O_3-targeting scheme can mitigate O_3 and fine particles simultaneously.

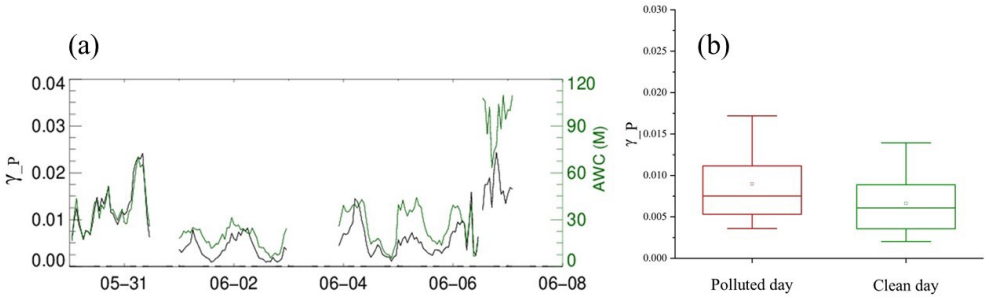

Figure 6. Results of N_2O_5 uptake coefficients through parameterization (γ_P). Panel **(a)** shows time series of γ_P and ISORROPIA II results of aerosol water content (AWC). Panel **(b)** is the box plot of the polluted days and clean days, the hollow square represents the mean value, and the solid line across the box shows the median score for the data set, while the top and bottom whiskers represent the 90 % and 10 % values of γ_P, respectively.

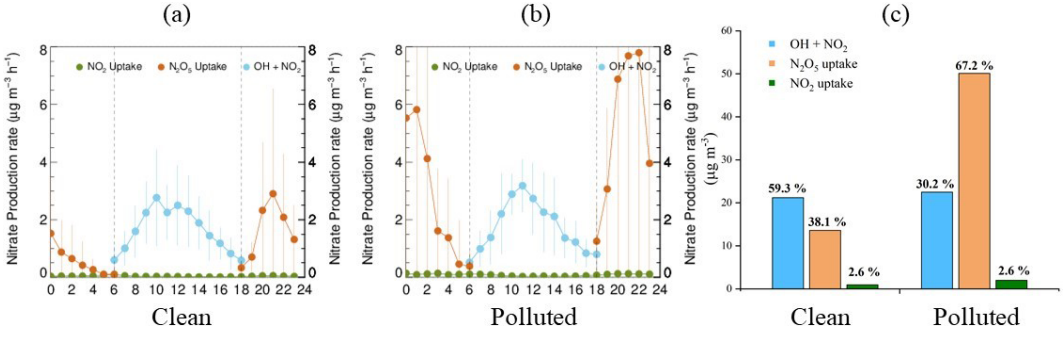

Figure 7. The mean diurnal variations of the nitrate production potential of clean days **(a)** and polluted days **(b)** and the $P(NO_3^-)$ distribution of clean days and polluted days **(c)**.

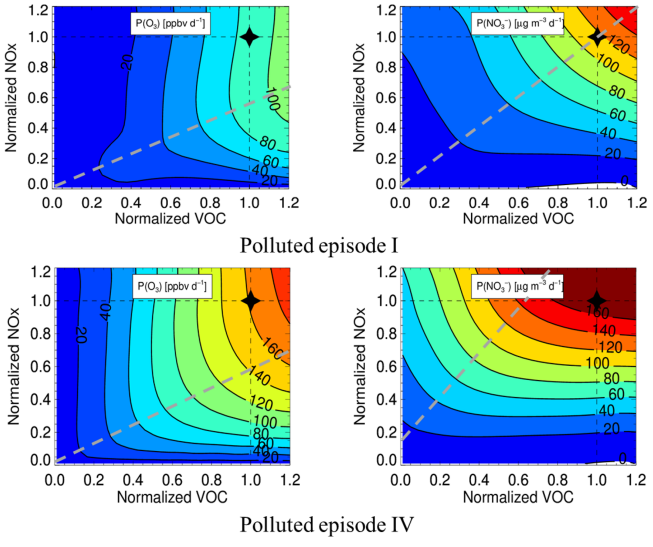

Figure 8. Isogram of $P(O_3)$ and $P(NO_3^-)$ of polluted episodes IV (30 May 2019 00:00–6 June 2019 00:00) and I (14 June 2019 17:30–17 June 2019 12:00) with different NO_x and VOC reduction degrees. The grey dashed line represents the ridge line.

4 Conclusions

A comprehensive campaign was conducted to interpret the atmospheric oxidation capacity and aerosol formation from 30 May to 18 June 2019 in Changzhou, China. The high O_3 and $PM_{2.5}$ concentrations confirm complex air pollution characteristics in Changzhou, and nitrate accounts for 38.3 % mass concentration of total water-soluble particulate components and 32.0 % of total $PM_{2.5}$. In addition, the average values of NOR are 0.32 on PDs and 0.25 on CDs. The positive correlation between NOR and RH and the inverse correlation refer to the contribution of N_2O_5 heterogeneous uptake to nitrate formation.

Based on field observations of OH and related parameters, we show that OH oxidation of the NO_2 pathway steadily contributes to nitrate formation no matter the clean or polluted period and dominates CD nitrate production (about 22 $\mu g\,m^{-3}$). N_2O_5 heterogeneous uptake contribution proliferated on polluted days, from 13.6 $\mu g\,m^{-3}$ (38.1 %) on clean days to 50.1 $\mu g\,m^{-3}$ (67.2 %) on polluted days. NO_2 heterogeneous uptake contributes little to nitrate formation (2.6 %).

The precursor reduction simulation suggests the reduction ratio of $VOC : NO_x$ equaling 2 : 1 can simultaneously and effectively mitigate O_3 and fine particle pollution during the summertime complex pollution period in Changzhou. To

more precisely and delicately establish a cooperative control scheme for regional O_3 and nitrate, the regional and long-time field campaigns are needed in the future to analyze the seasonal and interannual variation of O_3 and nitrate and relevant parameters.

Code and data availability. The data sets used in this study are available from the corresponding author upon request (k.lu@pku.edu.cn).

Author contributions. KL and YZ designed the study. TZ analyzed the data and wrote the paper with input from all the authors.

Competing interests. The contact author has declared that neither of the authors has any competing interests.

Disclaimer. Publisher's note: Copernicus Publications remains neutral with regard to jurisdictional claims in published maps and institutional affiliations.

Acknowledgements. Thanks for the data contributed by the field campaign team.

Financial support. This project is supported by the National Natural Science Foundation of China (grant nos. 21976006 and 42175111), the Beijing Municipal Natural Science Foundation for Distinguished Young Scholars (JQ19031), and the National Research Program for Key Issues in Air Pollution Control (DQGG0103-01, 2019YFC0214800).

Review statement. This paper was edited by Guangjie Zheng and reviewed by two anonymous referees.

References

Andreae, M. O., Schmid, O., Yang, H., Chand, D., Yu, J. Z., Zeng, L.-M., and Zhang, Y.-H.: Optical properties and chemical composition of the atmospheric aerosol in urban Guangzhou, China, Atmos. Environ., 42, 6335–6350, https://doi.org/10.1016/j.atmosenv.2008.01.030, 2008.

Bertram, T. H. and Thornton, J. A.: Toward a general parameterization of N_2O_5 reactivity on aqueous particles: the competing effects of particle liquid water, nitrate and chloride, Atmos. Chem. Phys., 9, 8351–8363, https://doi.org/10.5194/acp-9-8351-2009, 2009.

Bohn, B., Corlett, G. K., Gillmann, M., Sanghavi, S., Stange, G., Tensing, E., Vrekoussis, M., Bloss, W. J., Clapp, L. J., Kortner, M., Dorn, H.-P., Monks, P. S., Platt, U., Plass-Dülmer, C., Mihalopoulos, N., Heard, D. E., Clemitshaw, K. C., Meixner, F. X., Prevot, A. S. H., and Schmitt, R.: Photolysis frequency measurement techniques: results of a comparison within the ACCENT project, Atmos. Chem. Phys., 8, 5373–5391, https://doi.org/10.5194/acp-8-5373-2008, 2008.

Brown, S. S. and Stutz, J.: Nighttime radical observations and chemistry, Chem. Soc. Rev., 41, 6405–6447, https://doi.org/10.1039/c2cs35181a, 2012.

Brown, S. S., Stark, H., and Ravishankara, A. R.: Applicability of the steady state approximation to the interpretation of atmospheric observations of NO_3 and N_2O_5, J. Geophys. Res.-Atmos., 108, 5439, https://doi.org/10.1029/2003jd003407, 2003.

Brown, S. S., Dube, W. P., Fuchs, H., Ryerson, T. B., Wollny, A. G., Brock, C. A., Bahreini, R., Middlebrook, A. M., Neuman, J. A., Atlas, E., Roberts, J. M., Osthoff, H. D., Trainer, M., Fehsenfeld, F. C., and Ravishankara, A. R.: Reactive uptake coefficients for N_2O_5 determined from aircraft measurements during the Second Texas Air Quality Study: Comparison to current model parameterizations, J. Geophys. Res.-Atmos., 114, https://doi.org/10.1029/2008jd011679, 2009.

Cao, J.-J., Shen, Z.-X., Chow, J. C., Watson, J. G., Lee, S.-C., Tie, X.-X., Ho, K.-F., Wang, G.-H., and Han, Y.-M.: Winter and Summer $PM_{2.5}$ Chemical Compositions in Fourteen Chinese Cities, J. Air Waste. Manage., 62, 1214–1226, https://doi.org/10.1080/10962247.2012.701193, 2012.

Chan, Y. C., Evans, M. J., He, P. Z., Holmes, C. D., Jaegle, L., Kasibhatla, P., Liu, X. Y., Sherwen, T., Thornton, J. A., Wang, X., Xie, Z. Q., Zhai, S. T., and Alexander, B.: Heterogeneous Nitrate Production Mechanisms in Intense Haze Events in the North China Plain, J. Geophys. Res.-Atmos., 126, https://doi.org/10.1029/2021jd034688, 2021.

Chang, Y., Zhang, Y., Tian, C., Zhang, S., Ma, X., Cao, F., Liu, X., Zhang, W., Kuhn, T., and Lehmann, M. F.: Nitrogen isotope fractionation during gas-to-particle conversion of NO_x to NO_3^- in the atmosphere – implications for isotope-based NO_x source apportionment, Atmos. Chem. Phys., 18, 11647–11661, https://doi.org/10.5194/acp-18-11647-2018, 2018.

Chen, H., Hu, R., Xie, P., Xing, X., Ling, L., Li, Z., Wang, F., Wang, Y., Liu, J., and Liu, W.: A hydroxyl radical detection system using gas expansion and fast gating laser-induced fluorescence techniques, J. Environ. Sci., 65, 190–200, https://doi.org/10.1016/j.jes.2017.03.012, 2018.

Chen, X., Walker, J. T., and Geron, C.: Chromatography related performance of the Monitor for AeRosols and GAses in ambient air (MARGA): laboratory and field-based evaluation, Atmos. Meas. Tech., 10, 3893–3908, https://doi.org/10.5194/amt-10-3893-2017, 2017.

Chen, X., Wang, H., and Lu, K.: Interpretation of NO_3-N_2O_5 observation via steady state in high-aerosol air mass: the impact of equilibrium coefficient in ambient conditions, Atmos. Chem. Phys., 22, 3525–3533, https://doi.org/10.5194/acp-22-3525-2022, 2022.

Chen, X. R., Wang, H. C., Liu, Y. H., Su, R., Wang, H. L., Lou, S. R., and Lu, K. D.: Spatial characteristics of the nighttime oxidation capacity in the Yangtze River Delta, China, Atmos. Environ., 208, 150–157, https://doi.org/10.1016/j.atmosenv.2019.04.012, 2019.

Chen, X. R., Wang, H. C., Lu, K. D., Li, C. M., Zhai, T. Y., Tan, Z. F., Ma, X. F., Yang, X. P., Liu, Y. H., Chen, S. Y., Dong, H. B., Li, X., Wu, Z. J., Hu, M., Zeng, L. M., and Zhang, Y. H.: Field Determination of Nitrate Formation Path-

way in Winter Beijing, Environ. Sci. Technol., 54, 9243–9253, https://doi.org/10.1021/acs.est.0c00972, 2020.

Elshorbany, Y. F., Steil, B., Brühl, C., and Lelieveld, J.: Impact of HONO on global atmospheric chemistry calculated with an empirical parameterization in the EMAC model, Atmos. Chem. Phys., 12, 9977–10000, https://doi.org/10.5194/acp-12-9977-2012, 2012.

Fountoukis, C. and Nenes, A.: ISORROPIA II: a computationally efficient thermodynamic equilibrium model for K^+–Ca^{2+}–Mg^{2+}–NH_4^+–Na^+–SO_4^{2-}–NO_3^-–Cl–H_2O aerosols, Atmos. Chem. Phys., 7, 4639–4659, https://doi.org/10.5194/acp-7-4639-2007, 2007.

Goliff, W. S., Stockwell, W. R., and Lawson, C. V.: The regional atmospheric chemistry mechanism, version 2, Atmos. Environ., 68, 174–185, https://doi.org/10.1016/j.atmosenv.2012.11.038, 2013.

Guo, L., Hu, Y., Hu, Q., Lin, J., Li, C., Chen, J., Li, L., and Fu, H.: Characteristics and chemical compositions of particulate matter collected at the selected metro stations of Shanghai, China, Sci. Total Environ., 496, 443–452, https://doi.org/10.1016/j.scitotenv.2014.07.055, 2014.

Hagler, G. S. W., Bergin, M. H., Salmon, L. G., Yu, J. Z., Wan, E. C. H., Zheng, M., Zeng, L. M., Kiang, C. S., Zhang, Y. H., Lau, A. K. H., and Schauer, J. J.: Source areas and chemical composition of fine particulate matter in the Pearl River Delta region of China, Atmos. Environ., 40, 3802–3815, https://doi.org/10.1016/j.atmosenv.2006.02.032, 2006.

Jiang, M., Lu, K., Su, R., Tan, Z., Wang, H., Li, L., Fu, Q., Zhai, C., Tan, Q., Yue, D., Chen, D., Wang, Z., Xie, S., Zeng, L., and Zhang, Y.: Ozone formation and key VOCs in typical Chinese city clusters, Chinese Sci. Bull., 63, 1130–1141, 2018.

Kanaya, Y., Fukuda, M., Akimoto, H., Takegawa, N., Komazaki, Y., Yokouchi, Y., Koike, M., and Kondo, Y.: Urban photochemistry in central Tokyo: 2. Rates and regimes of oxidant ($O_3 + NO_2$) production, J. Geophys. Res.-Atmos., 113, https://doi.org/10.1029/2007jd008671, 2008.

Li, H., Zhang, Q., Zhang, Q., Chen, C., Wang, L., Wei, Z., Zhou, S., Parworth, C., Zheng, B., Canonaco, F., Prévôt, A. S. H., Chen, P., Zhang, H., Wallington, T. J., and He, K.: Wintertime aerosol chemistry and haze evolution in an extremely polluted city of the North China Plain: significant contribution from coal and biomass combustion, Atmos. Chem. Phys., 17, 4751–4768, https://doi.org/10.5194/acp-17-4751-2017, 2017.

Liu, X., Gu, J., Li, Y., Cheng, Y., Qu, Y., Han, T., Wang, J., Tian, H., Chen, J., and Zhang, Y.: Increase of aerosol scattering by hygroscopic growth: Observation, modeling, and implications on visibility, Atmos. Res., 132, 91–101, https://doi.org/10.1016/j.atmosres.2013.04.007, 2013.

Lou, S., Tan, Z., Gan, G., Chen, J., Wang, H., Gao, Y., Huang, D., Huang, C., Li, X., Song, R., Wang, H., Wang, M., Wang, Q., Wu, Y., and Huang, C.: Observation based study on atmospheric oxidation capacity in Shanghai during late-autumn: Contribution from nitryl chloride, Atmos. Environ., 271, 118902, https://doi.org/10.1016/j.atmosenv.2021.118902, 2022.

Lu, K. D., Rohrer, F., Holland, F., Fuchs, H., Bohn, B., Brauers, T., Chang, C. C., Häseler, R., Hu, M., Kita, K., Kondo, Y., Li, X., Lou, S. R., Nehr, S., Shao, M., Zeng, L. M., Wahner, A., Zhang, Y. H., and Hofzumahaus, A.: Observation and modelling of OH and HO_2 concentrations in the Pearl River Delta 2006: a missing OH source in a VOC rich atmosphere, Atmos. Chem. Phys., 12, 1541–1569, https://doi.org/10.5194/acp-12-1541-2012, 2012.

Lu, K. D., Hofzumahaus, A., Holland, F., Bohn, B., Brauers, T., Fuchs, H., Hu, M., Häseler, R., Kita, K., Kondo, Y., Li, X., Lou, S. R., Oebel, A., Shao, M., Zeng, L. M., Wahner, A., Zhu, T., Zhang, Y. H., and Rohrer, F.: Missing OH source in a suburban environment near Beijing: observed and modelled OH and HO_2 concentrations in summer 2006, Atmos. Chem. Phys., 13, 1057–1080, https://doi.org/10.5194/acp-13-1057-2013, 2013.

Ma, X., Tan, Z., Lu, K., Yang, X., Chen, X., Wang, H., Chen, S., Fang, X., Li, S., Li, X., Liu, J., Liu, Y., Lou, S., Qiu, W., Wang, H., Zeng, L., and Zhang, Y.: OH and HO_2 radical chemistry at a suburban site during the EXPLORE-YRD campaign in 2018, Atmos. Chem. Phys., 22, 7005–7028, https://doi.org/10.5194/acp-22-7005-2022, 2022.

Meng, Z. Y., Wu, L. Y., Xu, X. D., Xu, W. Y., Zhang, R. J., Jia, X. F., Liang, L. L., Miao, Y. C., Cheng, H. B., Xie, Y. L., He, J. J., and Zhong, J. T.: Changes in ammonia and its effects on $PM_{2.5}$ chemical property in three winter seasons in Beijing, China, Sci. Total Environ., 749, 142208, https://doi.org/10.1016/j.scitotenv.2020.142208, 2020.

Ming, L., Jin, L., Li, J., Fu, P., Yang, W., Liu, D., Zhang, G., Wang, Z., and Li, X.: $PM_{2.5}$ in the Yangtze River Delta, China: Chemical compositions, seasonal variations, and regional pollution events, Environ. Pollut., 223, 200–212, https://doi.org/10.1016/j.envpol.2017.01.013, 2017.

Phillips, G. J., Thieser, J., Tang, M., Sobanski, N., Schuster, G., Fachinger, J., Drewnick, F., Borrmann, S., Bingemer, H., Lelieveld, J., and Crowley, J. N.: Estimating N_2O_5 uptake coefficients using ambient measurements of NO_3, N_2O_5, $ClNO_2$ and particle-phase nitrate, Atmos. Chem. Phys., 16, 13231–13249, https://doi.org/10.5194/acp-16-13231-2016, 2016.

Qin, Y., Li, J. Y., Gong, K. J., Wu, Z. J., Chen, M. D., Qin, M. M., Huang, L., and Hu, J. L.: Double high pollution events in the Yangtze River Delta from 2015 to 2019: Characteristics, trends, and meteorological situations, Sci. Total Environ., 792, 148349, https://doi.org/10.1016/j.scitotenv.2021.148349, 2021.

Qiu, X., Ying, Q., Wang, S., Duan, L., Zhao, J., Xing, J., Ding, D., Sun, Y., Liu, B., Shi, A., Yan, X., Xu, Q., and Hao, J.: Modeling the impact of heterogeneous reactions of chlorine on summertime nitrate formation in Beijing, China, Atmos. Chem. Phys., 19, 6737–6747, https://doi.org/10.5194/acp-19-6737-2019, 2019.

Seinfeld, J. H. and Pandis, S. N.: Atmospheric chemistry and physics: from air pollution to climate change, 3rd, Book, Whole, Wiley, Hoboken, New Jersey, ISBN 978-1-118-94740-1, 2016.

Shang, D. J., Peng, J. F., Guo, S., Wu, Z. J., and Hu, M.: Secondary aerosol formation in winter haze over the Beijing-Tianjin-Hebei Region, China, Front. Env. Sci. Eng., 15, 1–13, https://doi.org/10.1007/s11783-020-1326-x, 2021.

Shu, L., Wang, T. J., Xie, M., Li, M. M., Zhao, M., Zhang, M., and Zhao, X. Y.: Episode study of fine particle and ozone during the CAPUM-YRD over Yangtze River Delta of China: Characteristics and source attribution, Atmos. Environ., 203, 87–101, https://doi.org/10.1016/j.atmosenv.2019.01.044, 2019.

Song, C. H. and Carmichael, G. R.: Gas-particle partitioning of nitric acid modulated by alkaline aerosol, J. Atmos. Chem., 40, 1–22, 2001.

Staudt, S., Gord, J. R., Karimova, N. V., McDuffie, E. E., Brown, S. S., Gerber, R. B., Nathanson, G. M., and Bertram, T. H.: Sulfate and Carboxylate Suppress the Formation of $ClNO_2$ at Atmospheric Interfaces, Acs Earth Space Chem., 3, 1987–1997, 2019.

Sun, Y. L., Zhuang, G. S., Tang, A. H., Wang, Y., and An, Z. S.: Chemical characteristics of $PM_{2.5}$ and PM_{10} in haze-fog episodes in Beijing, Environ. Sci. Technol., 40, 3148–3155, https://doi.org/10.1021/es051533g, 2006.

Tan, Z., Fuchs, H., Lu, K., Hofzumahaus, A., Bohn, B., Broch, S., Dong, H., Gomm, S., Häseler, R., He, L., Holland, F., Li, X., Liu, Y., Lu, S., Rohrer, F., Shao, M., Wang, B., Wang, M., Wu, Y., Zeng, L., Zhang, Y., Wahner, A., and Zhang, Y.: Radical chemistry at a rural site (Wangdu) in the North China Plain: observation and model calculations of OH,HO_2 and RO_2 radicals, Atmos. Chem. Phys., 17, 663–690, https://doi.org/10.5194/acp-17-663-2017, 2017.

Tan, Z., Lu, K. D., Dong, H. B., Hu, M., Li, X., Liu, Y. H., Lu, S. H., Shao, M., Su, R., Wang, H. C., Wu, Y. S., Wahner, A., and Zhang, Y. H.: Explicit diagnosis of the local ozone production rate and the ozone-NO_x-VOC sensitivities, Sci. Bull., 63, 1067–1076, https://doi.org/10.1016/j.scib.2018.07.001, 2018.

Tan, Z., Wang, H., Lu, K., Dong, H., Liu, Y., Zeng, L., Hu, M., and Zhang, Y.: An Observational Based Modeling of the Surface Layer Particulate Nitrate in the North China Plain During Summertime, J. Geophys. Res.-Atmos., 126, e2021JD035623, https://doi.org/10.1029/2021JD035623, 2021.

Tham, Y. J., Wang, Z., Li, Q., Wang, W., Wang, X., Lu, K., Ma, N., Yan, C., Kecorius, S., Wiedensohler, A., Zhang, Y., and Wang, T.: Heterogeneous N_2O_5 uptake coefficient and production yield of $ClNO_2$ in polluted northern China: roles of aerosol water content and chemical composition, Atmos. Chem. Phys., 18, 13155–13171, https://doi.org/10.5194/acp-18-13155-2018, 2018.

Wang, H. and Lu, K. D.: Determination and Parameterization of the Heterogeneous Uptake Coefficient of Dinitrogen Pentoxide (N_2O_5), Prog. Chem., 28, 917–933, https://doi.org/10.7536/pc151225, 2016.

Wang, H., Zhu, B., Shen, L., Xu, H., An, J., Pan, C., Li, Y. e., and Liu, D.: Regional Characteristics of Air Pollutants during Heavy Haze Events in the Yangtze River Delta, China, Aerosol Air Qual. Res., 16, 2159–2171, https://doi.org/10.4209/aaqr.2015.09.0551, 2016.

Wang, H., Lu, K., Chen, X., Zhu, Q., Chen, Q., Guo, S., Jiang, M., Li, X., Shang, D., Tan, Z., Wu, Y., Wu, Z., Zou, Q., Zheng, Y., Zeng, L., Zhu, T., Hu, M., and Zhang, Y.: High N_2O_5 Concentrations Observed in Urban Beijing: Implications of a Large Nitrate Formation Pathway, Environ. Sc. Tech. Lett., 4, 416–420, https://doi.org/10.1021/acs.estlett.7b00341, 2017a.

Wang, H., Chen, J., and Lu, K.: Development of a portable cavity-enhanced absorption spectrometer for the measurement of ambient NO_3 and N_2O_5: experimental setup, lab characterizations, and field applications in a polluted urban environment, Atmos. Meas. Tech., 10, 1465–1479, https://doi.org/10.5194/amt-10-1465-2017, 2017b.

Wang, H., Lu, K., Chen, X., Zhu, Q., Wu, Z., Wu, Y., and Sun, K.: Fast particulate nitrate formation via N_2O_5 uptake aloft in winter in Beijing, Atmos. Chem. Phys., 18, 10483–10495, https://doi.org/10.5194/acp-18-10483-2018, 2018a.

Wang, H., Lu, K., Guo, S., Wu, Z., Shang, D., Tan, Z., Wang, Y., Le Breton, M., Lou, S., Tang, M., Wu, Y., Zhu, W., Zheng, J., Zeng, L., Hallquist, M., Hu, M., and Zhang, Y.: Efficient N_2O_5 uptake and NO_3 oxidation in the outflow of urban Beijing, Atmos. Chem. Phys., 18, 9705–9721, https://doi.org/10.5194/acp-18-9705-2018, 2018b.

Wang, H., Chen, X. R., Lu, K. D., Hu, R. Z., Li, Z. Y., Wang, H. L., Ma, X. F., Yang, X. P., Chen, S. Y., Dong, H. B., Liu, Y., Fang, X., Zeng, L. M., Hu, M., and Zhang, Y. H.: NO_3 and N_2O_5 chemistry at a suburban site during the EXPLORE-YRD campaign in 2018, Atmos. Environ., 224, 117180, https://doi.org/10.1016/j.atmosenv.2019.117180, 2020a.

Wang, H., Chen, X. R., Lu, K. D., Tan, Z. F., Ma, X. F., Wu, Z. J., Li, X., Liu, Y. H., Shang, D. J., Wu, Y. S., Zeng, L. M., Hu, M., Schmitt, S., Kiendler-Scharr, A., Wahner, A., and Zhang, Y. H.: Wintertime N_2O_5 uptake coefficients over the North China Plain, Sci. Bull., 65, 765–774, https://doi.org/10.1016/j.scib.2020.02.006, 2020b.

Wang, S. B., Wang, L. L., Fan, X. G., Wang, N., Ma, S. L., and Zhang, R. Q.: Formation pathway of secondary inorganic aerosol and its influencing factors in Northern China: Comparison between urban and rural sites, Sci. Total Environ., 840, 156404, https://doi.org/10.1016/j.scitotenv.2022.156404, 2022.

Wang, X. F., Zhang, Y. P., Chen, H., Yang, X., Chen, J. M., and Geng, F. H.: Particulate Nitrate Formation in a Highly Polluted Urban Area: A Case Study by Single-Particle Mass Spectrometry in Shanghai, Environ. Sci. Technol., 43, 3061–3066, 2009.

Wang, Z., Wang, W., Tham, Y. J., Li, Q., Wang, H., Wen, L., Wang, X., and Wang, T.: Fast heterogeneous N_2O_5 uptake and $ClNO_2$ production in power plant and industrial plumes observed in the nocturnal residual layer over the North China Plain, Atmos. Chem. Phys., 17, 12361–12378, https://doi.org/10.5194/acp-17-12361-2017, 2017.

Woodward-Massey, R., Slater, E. J., Alen, J., Ingham, T., Cryer, D. R., Stimpson, L. M., Ye, C., Seakins, P. W., Whalley, L. K., and Heard, D. E.: Implementation of a chemical background method for atmospheric OH measurements by laser-induced fluorescence: characterisation and observations from the UK and China, Atmos. Meas. Tech., 13, 3119–3146, https://doi.org/10.5194/amt-13-3119-2020

Wu, S. P., Dai, L. H., Zhu, H., Zhang, N., Yan, J. P., Schwab, J. J., and Yuan, C. S.: The impact of sea-salt aerosols on particulate inorganic nitrogen deposition in the western Taiwan Strait region, China, Atmos. Res., 228, 68–76, 2019.

Xia, M., Peng, X., Wang, W., Yu, C., Sun, P., Li, Y., Liu, Y., Xu, Z., Wang, Z., Xu, Z., Nie, W., Ding, A., and Wang, T.: Significant production of ClNO2 and possible source of Cl_2 from N_2O_5 uptake at a suburban site in eastern China, Atmos. Chem. Phys., 20, 6147–6158, https://doi.org/10.5194/acp-20-6147-2020, 2020.

Xu, J. W., Huang, X., Wang, N., Li, Y. Y., and Ding, A. J.: Understanding ozone pollution in the Yangtze River Delta of eastern China from the perspective of diurnal cycles, Sci. Total Environ., 752, 141928, https://doi.org/10.1016/j.scitotenv.2020.141928, 2021.

Xue, H., Liu, G., Zhang, H., Hu, R., and Wang, X.: Similarities and differences in PM_{10} and $PM_{2.5}$ concentrations, chemical compositions and sources in Hefei City, China, Chemosphere, 220, 760–765, https://doi.org/10.1016/j.chemosphere.2018.12.123, 2019.

Yang, X. P., Lu, K. D., Ma, X. F., Liu, Y. H., Wang, H. C., Hu, R. Z., Li, X., Lou, S. R., Chen, S. Y., Dong, H. B., Wang, F. Y., Wang,

Y. H., Zhang, G. X., Li, S. L., Yang, S. D., Yang, Y. M., Kuang, C. L., Tan, Z. F., Chen, X. R., Qiu, P. P., Zeng, L. M., Xie, P. H., and Zhang, Y. H.: Observations and modeling of OH and HO_2 radicals in Chengdu, China in summer 2019, Sci. Total Environ., 772, 144829, https://doi.org/10.1016/j.scitotenv.2020.144829, 2021.

Yu, C., Wang, Z., Xia, M., Fu, X., Wang, W., Tham, Y. J., Chen, T., Zheng, P., Li, H., Shan, Y., Wang, X., Xue, L., Zhou, Y., Yue, D., Ou, Y., Gao, J., Lu, K., Brown, S. S., Zhang, Y., and Wang, T.: Heterogeneous N_2O_5 reactions on atmospheric aerosols at four Chinese sites: improving model representation of uptake parameters, Atmos. Chem. Phys., 20, 4367–4378, https://doi.org/10.5194/acp-20-4367-2020, 2020.

Yu, C. A., Wang, Z., Ma, Q. X., Xue, L. K., George, C., and Wang, T.: Measurement of heterogeneous uptake of NO_2 on inorganic particles, sea water and urban grime, J. Environ. Sci., 106, 124–135, https://doi.org/10.1016/j.jes.2021.01.018, 2021.

Yu, D., Tan, Z., Lu, K., Ma, X., Li, X., Chen, S., Zhu, B., Lin, L., Li, Y., Qiu, P., Yang, X., Liu, Y., Wang, H., He, L., Huang, X., and Zhang, Y.: An explicit study of local ozone budget and NO_x-VOCs sensitivity in Shenzhen China, Atmos. Environ., 224, 117304, https://doi.org/10.1016/j.atmosenv.2020.117304, 2020.

Zhang, K., Xu, J. L., Huang, Q., Zhou, L., Fu, Q. Y., Duan, Y. S., and Xiu, G. L.: Precursors and potential sources of ground-level ozone in suburban Shanghai, Front. Env. Sci. Eng., 14, https://doi.org/10.1007/s11783-020-1271-8, 2020.

Zhang, R., Han, Y. H., Shi, A. J., Sun, X. S., Yan, X., Huang, Y. H., and Wang, Y.: Characteristics of ambient ammonia and its effects on particulate ammonium in winter of urban Beijing, China, Environ. Sci. Pollut. R, 28, 62828–62838, 2021.

Zhang, Y., Tang, L., Yu, H., Wang, Z., Sun, Y., Qin, W., Chen, W., Chen, C., Ding, A., Wu, J., Ge, S., Chen, C., and Zhou, H.-C.: Chemical composition, sources and evolution processes of aerosol at an urban site in Yangtze River Delta, China during wintertime, Atmos. Environ., 123, 339–349, https://doi.org/10.1016/j.atmosenv.2015.08.017, 2015.

Zhang, Y., Tang, L., Croteau, P. L., Favez, O., Sun, Y., Canagaratna, M. R., Wang, Z., Couvidat, F., Albinet, A., Zhang, H., Sciare, J., Prévôt, A. S. H., Jayne, J. T., and Worsnop, D. R.: Field characterization of the $PM_{2.5}$ Aerosol Chemical Speciation Monitor: insights into the composition, sources, and processes of fine particles in eastern China, Atmos. Chem. Phys., 17, 14501–14517, https://doi.org/10.5194/acp-17-14501-2017, 2017.

Zhang, Y., Hong, Z., Chen, J., Xu, L., Hong, Y., Li, M., Hao, H., Chen, Y., Qiu, Y., Wu, X., Li, J.-R., Tong, L., and Xiao, H.: Impact of control measures and typhoon weather on characteristics and formation of $PM_{2.5}$ during the 2016 G20 summit in China, Atmos. Environ., 224, 117312, https://doi.org/10.1016/j.atmosenv.2020.117312, 2020.

Zhang, Y. Y., Tang, A. H., Wang, C., Ma, X., Li, Y. Z., Xu, W., Xia, X. P., Zheng, A. H., Li, W. Q., Fang, Z. G., Zhao, X. F., Peng, X. L., Zhang, Y. P., Han, J., Zhang, L. J., Collett, J. L., and Liu, X. J.: $PM_{2.5}$ and water-soluble inorganic ion concentrations decreased faster in urban than rural areas in China, J. Environ. Sci., 122, 83–91, 2022.

Zhao, P. S., Dong, F., He, D., Zhao, X. J., Zhang, X. L., Zhang, W. Z., Yao, Q., and Liu, H. Y.: Characteristics of concentrations and chemical compositions for $PM_{2.5}$ in the region of Beijing, Tianjin, and Hebei, China, Atmos. Chem. Phys., 13, 4631–4644, https://doi.org/10.5194/acp-13-4631-2013, 2013.

Zhao, Z. Z., Sun, N., Zhou, W. L., Ma, S. S., Li, X. D., Li, M. L., Zhang, X., Tang, S. S., and Ye, Z. L.: Chemical Compositions in Winter $PM_{2.5}$ in Changzhou of the Yangtze River Delta Region, China: Characteristics and Atmospheric Responses Along With the Different Pollution Levels, Front. Env. Sci.-Switz, 10, 907735, https://doi.org/10.3389/fenvs.2022.907735, 2022.

Zheng, G. J., Duan, F. K., Su, H., Ma, Y. L., Cheng, Y., Zheng, B., Zhang, Q., Huang, T., Kimoto, T., Chang, D., Pöschl, U., Cheng, Y. F., and He, K. B.: Exploring the severe winter haze in Beijing: the impact of synoptic weather, regional transport and heterogeneous reactions, Atmos. Chem. Phys., 15, 2969–2983, https://doi.org/10.5194/acp-15-2969-2015, 2015.